Third Harmonic Shear Horizontal Waves for Material Degradation Monitoring

Fuzhen Wen, Shengbo Shan and Li Cheng

Department of mechanical engineering, The Hong Kong Polytechnic University, Kowloon, Hong Kong.

The Hong Kong Polytechnic University Shenzhen Research Institute, Shenzhen 518057, China.

Hong Kong Branch of National Rail Transit Electrification and Automation Engineering Technology Research Center, The Hong Kong Polytechnic University, Kowloon, Hong Kong.

E-mail: li.cheng@polyu.edu.hk

Abstract

Early detection of incipient damage in structures through material degradation monitoring is a challenging and important topic. Nonlinear guided waves, through their interaction with material micro-defects, allow possible detection of structural damage at its early stage of initiations. This issue is investigated using both the second harmonic Lamb (2^{nd} Lamb) waves and the third harmonic shear horizontal (3^{rd} SH) waves in this paper. A brief analysis first highlights the selection of the primary-secondary S0 Lamb wave mode pair and primary-tertiary SH0 mode pair from the perspective of cumulative high order harmonic wave generation. Through a tactic design, an experiment is then conducted to compare the sensitivity of the 3^{rd} SH waves and the 2^{nd} Lamb waves to microstructural changes on the same plate subjected to a dedicated thermal heating treatment. The 3^{rd} SH waves are finally applied to monitor the microstructural changes and material degradation in a plate subjected to a thermal aging sequence, cross-checked by Vickers Hardness tests. The experiment results demonstrate that the 3^{rd} SH waves indeed exhibit higher sensitivity to

microstructural changes than the commonly used 2nd Lamb waves. In addition, results demonstrate that the designed 3rd SH-wave-based system entails effective characterization of thermal-aging induced microstructural changes in metallic plates.

Keywords Third harmonic SH waves, Microstructural changes, Thermal aging, Material nonlinearity of plate, Vickers Hardness tests

1. INTRODUCTION

Early-stage material degradation in engineering structures, manifested in various forms such as thermal aging, fatigue, plastic deformation and micro cracks etc., can gradually evolve into macro damage so as to lead to prompt structural failure [1-4]. Therefore, their early detection is vital for facilitating timely maintenance decisions. Among existing damage detection techniques, the one based on nonlinear elastic waves has been attracting wide attentions [5-7]. Specifically, for thin-walled structures such as plates, the second harmonic Lamb waves (2nd Lamb waves) have been extensively explored and applied for the characterization of material degradation during the process of fatigue [8, 9], plastic deformation, [10] and thermal aging [11], etc.

Recently, the 3rd SH waves were shown to offer appealing features for damage detection in plates [12-14]. Due to their distinct features, SH waves are internally resonant with their third harmonic counterparts at all frequencies [14], which offers enormous flexibility for the selection of the excitation frequency in the design of inspection systems. Second, as claimed by Liu *et al.* [15], the 3rd SH waves seem to exhibit a higher sensitivity to plastic (fatigue) deformation than the commonly used 2nd Lamb waves, thus pointing at the possibility of shifting the detection limit to the earlier stage. However, the reported

sensitivity comparison between the 3rd SH waves and the 2nd Lamb waves was conducted using two different test specimens and experimental configurations [10, 15]. In order to draw a more convincing and quantitative conclusion, more rigorous comparative experiment is needed. The issue, however, is technically challenging because of the difficulty in coping with the non-damage-related nonlinear sources existing in a test system whose influence might overwhelm the damage-related nonlinear components. Therefore, a meaningful comparative experiment can only be materialized after the undesired nonlinear sources are meticulously mitigated. On the top of this is the prerequisite of generating both well-controlled SH and Lamb waves on the same test sample, which requires meticulous care as well.

Motivated by this, this paper reports a systematic investigation on the 3rd SH waves in the perspective of monitoring the incipient microstructural changes inside a metallic structure, exemplified by a thermal-aging-induced material degradation. Particular attention is paid to acquiring a quantitative comparison of their detection sensitivity with the commonly used 2nd Lamb waves using a meticulously designed experimental configuration. To facilitate the analysis, the mechanism behind both the second harmonic and third harmonic generation in a nonlinear material is first brievely revisited. The primary-secondary S0 Lamb wave mode pair and the primary-tertiary SH0 mode pair are selected based on the cumulative feature of their nonlinear components. Then, a preheated specimen is choosen as a benchmark to carry out a comparative experiment, in which the sensitivity of the 2nd S0 mode Lamb waves and that of the 3rd SH0 mode SH waves to microstructural changes subject to a dedicated thermal heating treatment on the same plate are compared. To make this possible, the system is tactically designed to ensure dominant

material nonlinearity over other non-damage related nonlinear sources. Finally, the 3rd SH waves are applied to monitor the microstructural changes and material degradation in a metal plate after imposing a sequence of thermal aging treatment. The measured variation trends using the 3rd SH waves are further confirmed and validated by the Vickers Hardness tests.

2. EXPERIMENTAL DESIGN

2.1 Theoretical background

To provide guidance to the experimental design, the mechanism of the 2nd Lamb wave and the 3rd SH wave generation is brievely revisited. For the former, exisiting literature [16] shows that the primary S0-secondary S0 Lamb wave mode pair can approximately satisfy the synchronization conditions in the relatively low-frequency range, resulting in the quasi-cumulative second harmonic generation. As such, this specific mode pair offers great flexibility for the choice of excitation frequencies as only slight wave dispersion exists. In light of this, the primary S0-secondary S0 mode pair is used in this work. For the latter, it is known that the 3rd SH waves are cumulative at all frequencies [17], which ensures a strong third harmonic SH wave amplitude after a certain propagating distance, thus facilitating its quantification through measurement. As a typical example, the primary SH0-tertiary SH0 mode pair will be used in the subsquent experiments.

Besides, it is worth noting that the 2nd Lamb waves generated by the primary Lamb waves and the 3rd SH waves by the primary SH waves are determined by the Landau constants. Specifically, the former is tied with the TOECs while the latter to both TOECs

and FOECs [17]. Therefore, incipient damage like thermal damage leads to material microstructural changes, which can be reflected by the changes in the higher-order elastic constants and consequently the corresponding nonlinear Lamb waves and SH wave responses.

2.2 Specimen and preheating treatment

A comparative experiment is first conducted on a 2mm-thick 2024-T3 plate, which is a wrought heat-treatable Al-Cu-Mg alloy. As a typical type of material degradation, microstructural changes due to thermal aging are considered for threefold reasons: 1). It is indeed a damage type relevant to many industrial applications; 2). it is relatively easy to control the damage level and size through heating; and 3). It represents a weak incipient damage scenario, conducive to the quantification of the sensitivity of the detection methods. To create material property changes in the plate, a specially designed thermal treatment is applied. Over the thermal aging process, the precipitation sequence along dislocations is known as SSS→GPB→S"→S'→S [18]. As the main precipitate, S phase (Al_2CuMg) precipitation becomes coarse over the thermal aging process, leading to a significant microstructural change in the material [19]. The variations in the dislocation density associated with the dislocation pileups at precipitates and grain boundaries should sufficiently affect the generation of higher harmonic ultrasonic waves [15,20].

The microstructural changes induced by the precipitation can be manually controlled by deploying different heating schemes. In this specific case, the central zone of the plate is preheated for 3 hours at 200℃. According to the curves showing the effect of aging

temperatures on the age-hardening of Aluminum 2024-T3 alloy (without external stress) given in [18], the material in the heating zone enters an over-aging state after the preheating treatment. This stage is referred to as “State 1”, as shown in Fig. 1(a). As demonstrated in a previous study [16], this preheating would have already created significant microstructures inside the plate. After that, subsquent thermal treatment is carried out again at the same temperature for another 2 hours to reach the “State 2”. For the Aluminum 2024-T3 specimen used in this work, it has been shown that the microstructures in the plate change significantly when subject to the initial heating, but only slightly during the subsequent reheating process [21]. It is worth noting that the sensitivity comparison was made with respect ot the thermally-aged plate at State 1 and State 2. The rationale behind the deliberate design of such an experimental campaign is to be able to test the sensitivity of both methods in detecting small and incremental microstructural changes inside the plate due to further heating.

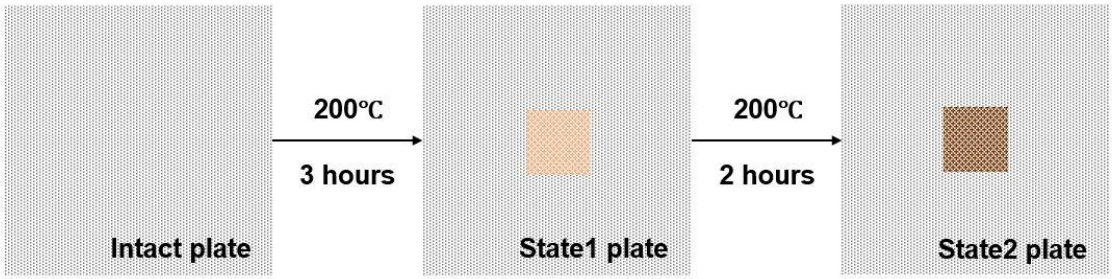

(a)

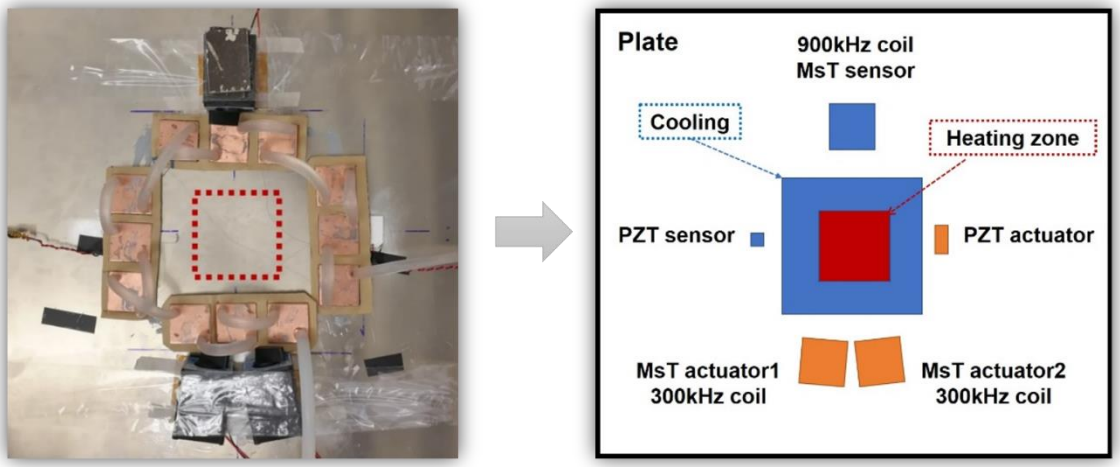

(b)

Figure 1. (a) Heating process for ultrasonic tests; (b) sketch of the Experimental set-up.

2.3 Experimental set-up

The experimental set-up is illustrated in Fig. 1(b). The thermal treatment on the aluminum plate is achieved by a temperature-control heating platform within a $100\text{mm} \times 100\text{mm}$ heating area. A cooling system is used to produce a barrier to prevent the heat transfer from the heating area to the transducer-bonding areas. The cooling system comprises 12 cooper blocks with cooling water passing through. Consequently, the

transducer-bonding areas remain at less than 50°C during the entire heating process, which should have negligible effect on the properties of transducers and adhesive layers.

In the experiments, magnetostrictive transducers (MsTs) and piezoelectric transducers (PZTs) are used for the generation and the reception of SH waves and Lamb waves, respectively. The MsT-activated system and the PZT-activated system are installed on the plate simultaneously. The former contains two MsT actuators and one MsT sensor for SH waves. Each actuator has a 5-fold coil with a 5.4mm gap, corresponding to the half wavelength of the 300kHz SH0 waves in the plate. In contrast, the sensor has a 5-fold coil with a 1.8mm gap, designed to be sensitive to the 900kHz SH0 waves. As demonstrated in the previous study [22], the nonlinearity from the transducers and instruments generally overwhelms that of the material nonlinearity from the aluminum plate. That is the reason why two MsT actuators are used. Through a subtraction signal separation scheme [17,23] with two independent channels of the RITEC RAM-5000-SHAP system, the nonlinearity of the MsT actuators can be effectively eliminated so that the damage-related nonlinear responses can be effectively acquired. A 12-cycle tone-burst pulse with a central frequency of 300kHz is used for excitations. For Lamb waves, one PZT actuator and one PZT sensor are used for the wave generation and reception, respectively. Based on a previous work [15], the system configuration is carefully designed to mitigate the influence of the un-damage-related adhesive nonlinearity (AN). Specifically, an 18-mm wide PZT actuator is used for the excitation of primary S0 mode Lamb waves at 160 kHz. Measurements are made with the National Instrument (NI) system, with details described in [15]. In each test, 200 signals are averaged to minimize the influence of the measurement noise.

3. SENSITIVITY COMPARISON BETWEEN 3RD SH WAVES AND 2ND LAMB WAVES

3.1 SH wave results from MsT-activated SHM system

In the MsT-activated SHM system, when the actuators of both channels were activated simultaneously, the overall responses at Intact state, State 1 and State 2 are shown in Fig. 2. Through calculating and checking the group velocities, the dominant wave packets are confirmed to correspond to the SH0 waves. No obvious difference can be observed between the three signals, demonstrating the limitation of linear ultrasonic-wave-based method for the detection of microstructural changes.

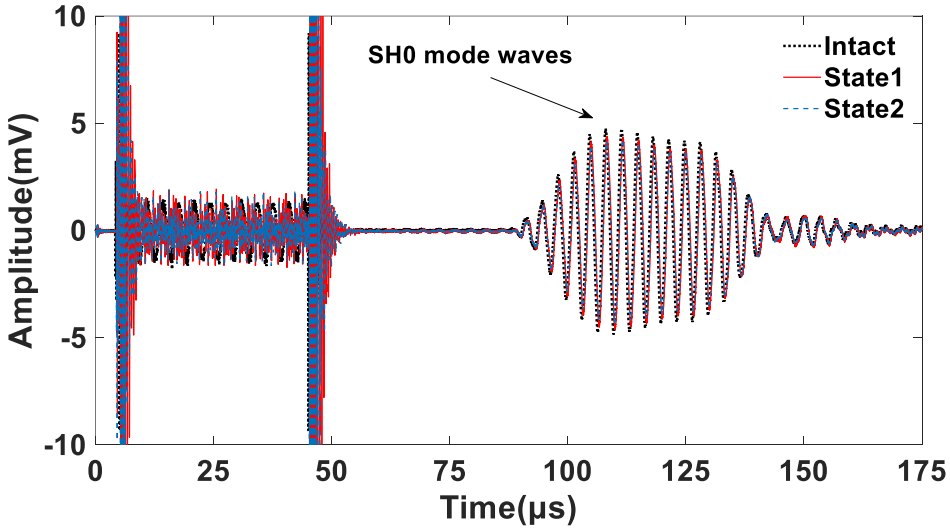

Figure 2. Overall signals at three states captured in the MsT-activated SHM system.

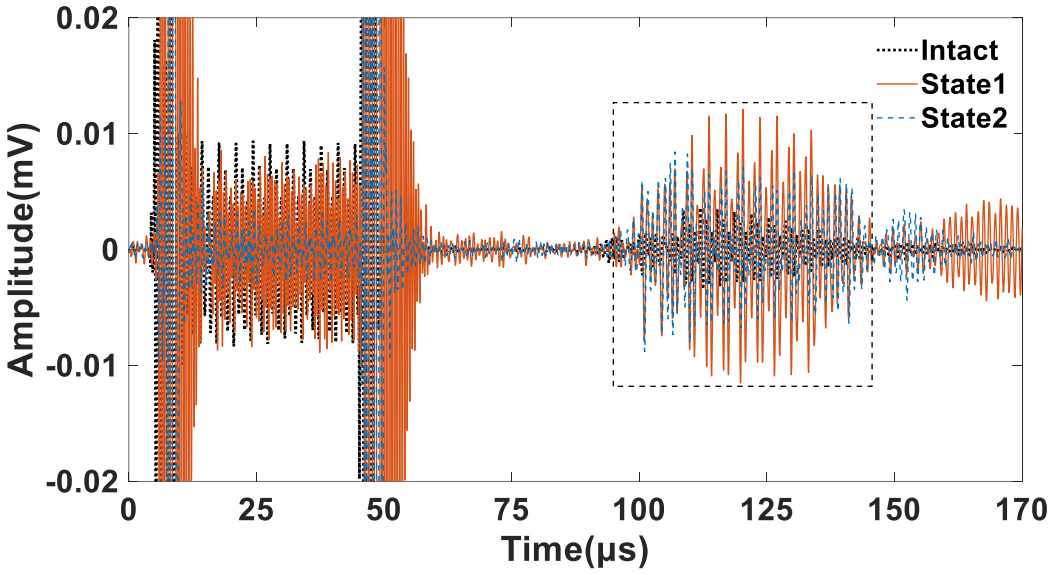

(a)

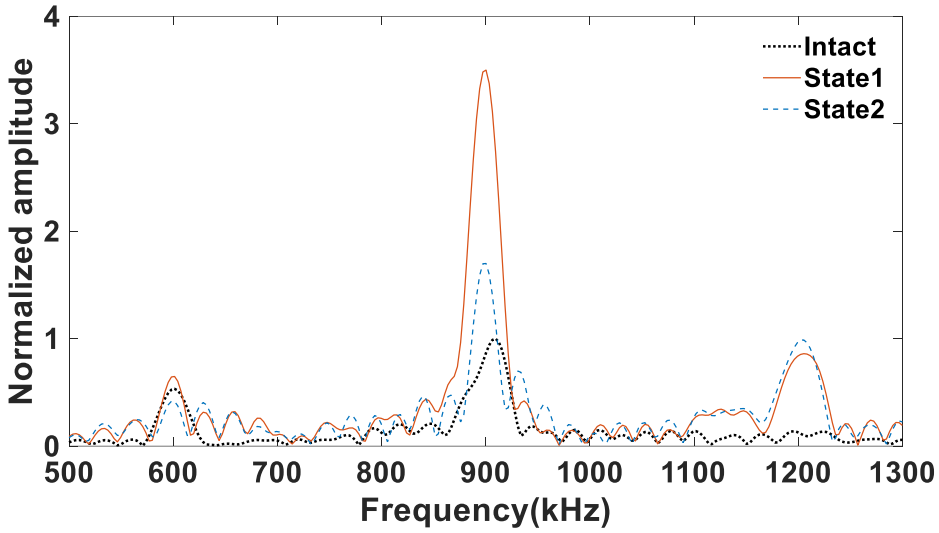

(b)

Figure 3. (a) extracted time-domain nonlinear responses associated with the three material stages:

(b) spectra of the windowed wave packets in (a).

The responses separately excited from the two transducers are denoted as $T(1)$ and $T(2)$, respectively. Accordingly, $T(1+2)$ represents the mixed responses when the two transducers are simultaneously activated. Taking the subtraction method to extract the nonlinear wave components as $R_{NL} = T(1+2) - T(1) - T(2)$, the influence of nonlinear sources from the actuator components can be eliminated. As shown in Fig. 3(a), the processed nonlinear responses of the three tests, corresponding to the Intact state, State 1 and State 2 of the material, are two orders of magnitude smaller than the overall responses presented in Fig. 2. Once applying the FFT to the windowed wave packets in Fig. 3(a), significant third harmonic responses can be clearly observed in Fig. 3(b). It can be seen that, the amplitude of the third harmonic wave component at around 900kHz experiments experiences a dramatic increase (356%) after the preheating process, indicating the significant changes in terms of material nonlinearities from Intact state to State 1. After that, a remarkable reduction (more than 50%) can be observed when the material transforms from State 1 to State 2. Such a roller coaster-like variation should only be attributed to the microstructural changes in the material induced by two thermal treatments.

3.2 Lamb wave results from the PZT-activated SHM system

Similarly, the overall responses acquired in the PZT-activated system at the three states are shown in Fig. 4. Again, no noticeable change can be observed in the linear responses. Upon using the previously developed superposition method [15], the second harmonic components are extracted using the responses to a pair of excitation signals with inversed phase, as shown in Fig. 5(a). With the specifically-designed system, the wave packets in

the dotted window are associated with the 2nd Lamb waves where the material nonlinearity dominates. The magnitude information of the second harmonic responses in the window shows a large difference before and after the heating treatments. Furthermore, the FFT mothed is applied to the windowed wave packtets in Fig. 5(a). The corresponding frequency domain responses of the three states are shown in Fig. 5(b). Similarly, the amplitude of the second harmonic wave component at around 320kHz is increased more than two times from Intact state to State 1. This validates the efficient of the optimimun design for the PZT-activated system again when the only variable is the material state changed by the thermal treatment. By contrast, results show a very slight reduction (2.2%) after the re-heating process. This confirms that the 2nd Lamb waves are not sensitive enough to detect the microstructural changes from State1 to State 2.

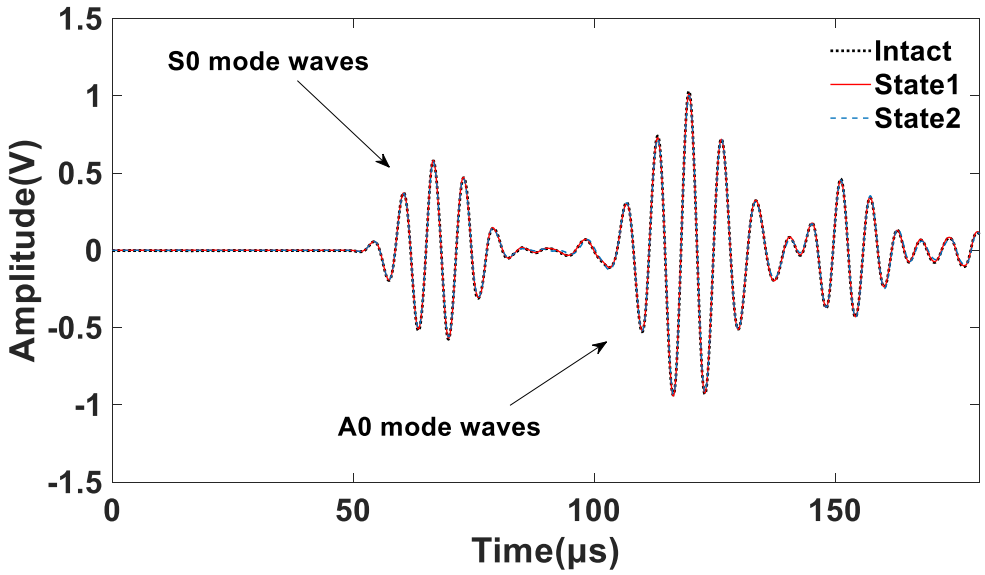

Figure 4. Overall signals at three states captured in the PZT-activated SHM system.

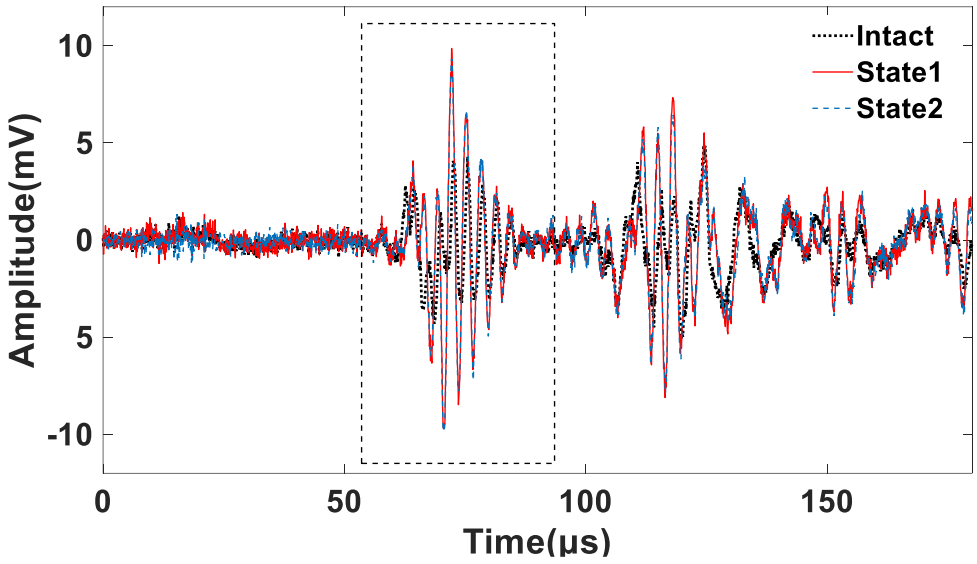

(a)

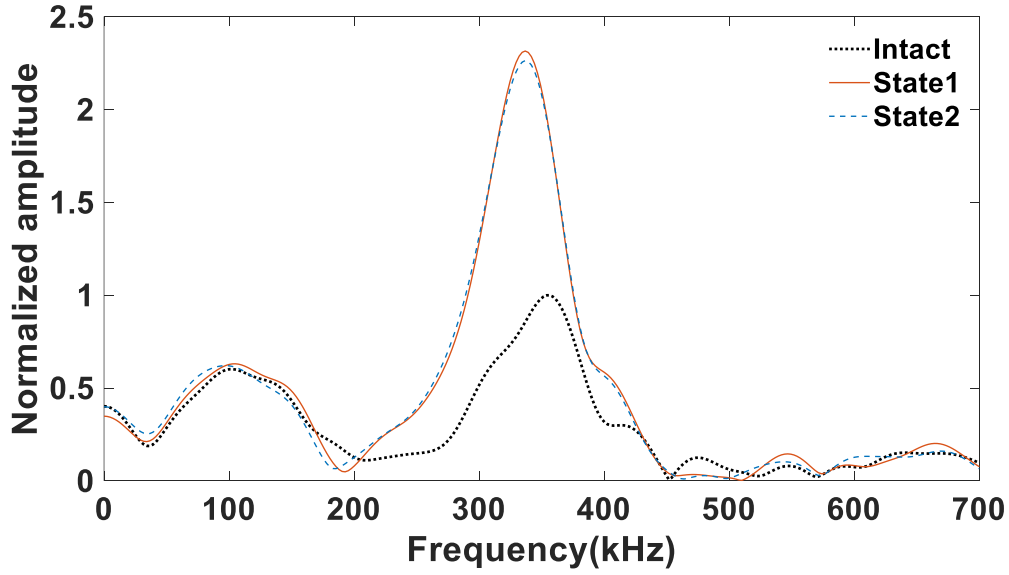

(b)

Figure 5. (a) 2nd Lamb wave responses corresponding to the two material stages; (b) spectra of the windowed wave packets in (a).

Through comparing the results in Fig. 3(b) and Fig. 5(b) for the same damage scenario in the same plate, it is clear that the 3rd SH waves exhibit much higher sensitivity to the microstructural changes than the 2nd Lamb waves since the material microstructures undergo the same change in the same test sample and using the same measurement systems. This confirms the superiority of the 3rd SH waves for early damage detection.

The experimental results point to the need for a closer examination on the correlation between the thermal-induced microstructural changes and the high order material elastic constants which affect the generation of high order harmonics as mentioned in the theoretical part. Considering the large vagaries of possible incipient damage forms and the corresponding microstructures, it might be virtually impossible to set up a direct and universal link between the microstructures of different damages to the Landau higher-order elastic constants used in this work. Nevertheless, an analysis on a parallel one-dimensional problem could allow better understanding on the obtained experimental results. This is done in Appendix through examining the relationship between a typical microstructural change (dislocation) and the higher-order elastic constants. By extending an existing dislocation model to a higher order one, it is demonstrated that the third order elastic constant is proportional to the dislocation density while the fourth order one to its square. For scenarios in which an incipient damage increases the dislocation density, the fourth order elastic constant should, in principle, be more sensitive to the dislocation variation caused by incipient damage than the third order one. Recalling the statements in the theoretical analyses, the generated 2nd Lamb waves are only related to the TOECs while the generated 3rd SH waves to both TOECs and FOECs in a weakly nonlinear plate. In

analogy with the 1D case (though the wave pattern being different), it is deduced the experimentally observed higher sensitivity of the 3rd SH waves is not accidental.

4. MONITORING OF MICROSTRUCTURAL CHANGES IN THERMALLY AGED PLATES USING THE 3RD SH WAVES

4.1 Experimental strategy

After demonstrating the high sensitivity of the 3rd SH waves to the microstructural changes from the experimental perspectives, they are further applied to monitor the evolution of the material degradation in a plate following a specific thermal aging process. In the experiment, the same MsT-activated SHM system as that used in the previous section is installed on a 2024-T3 plate of $625\text{mm} \times 625\text{mm} \times 2\text{mm}$ in size, as shown in Fig. 6(a). A heating sequence is designed in Fig. 6(b) to generate a continuous change of the microstructure inside the plate. Test using SH waves is carried out before heating the plate, which is referred to as the intact case. Then, the central area of the plate is heated to 200°C for an hour with the installation of the heat barriers, same as [17]. After cooling down to the room temperature and removing the heat barriers, test is carried out again to capture the primary and high order harmonic responses. Such process is then repeated for three more times with 2-hour, 3-hour and 4-hour heating time respectively. It is worth noting that the cooling time should not affect test results.

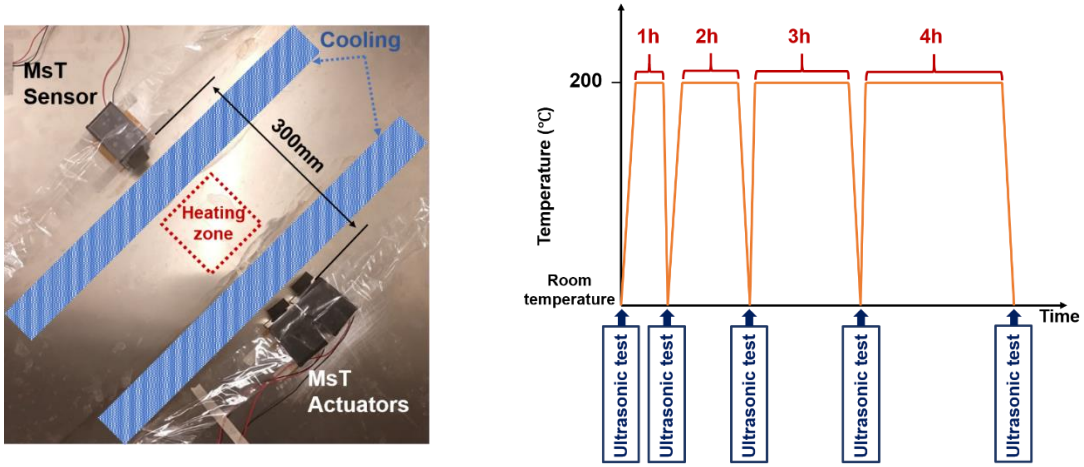

(a) (b)

Figure 6. (a) Set-up of a MsT-activated SHM system; (b) heating scheme of thermal aging treatment.

According to the literature [25], the second phase precipitation in the material has high correlation with the hardness of the heat-treatable 2024-T3 alloy. Therefore, a Vickers hardness test is also carried out at each heating stage as shown in Fig. 6(b) to cross-check with the ultrasonic test results.

4.2 Results and discussions

The nonlinear SH responses are extracted using the same subtraction method described in the previous section. Following the same procedure, FFT analysis is applied to extract the amplitude of the frequency response. To ensure a high repeatability of the results, the same tests are repeated four times to calculate the error bars. After normalization with

respect to the intact case, the third harmonic SH wave amplitudes corresponding to different heating hours are obtained and shown in Fig. 7(a). In this figure, the horizontal axis represents the cumulative heating time. It can be seen that, after one-hour heating, a dramatic increase (120%) in the nonlinear responses can be observed. Besides, during the first 3 hours, the amplitude of the 3rd harmonic SH wave increases rapidly, roughly up to two times of that in the intact case. After that, an obvious amplitude reduction takes place. This implies the material microstructures become stable after a total of 6-hour heating. This similar decrease trend can also be observed in the comparative tests as described in the Section 3.2.

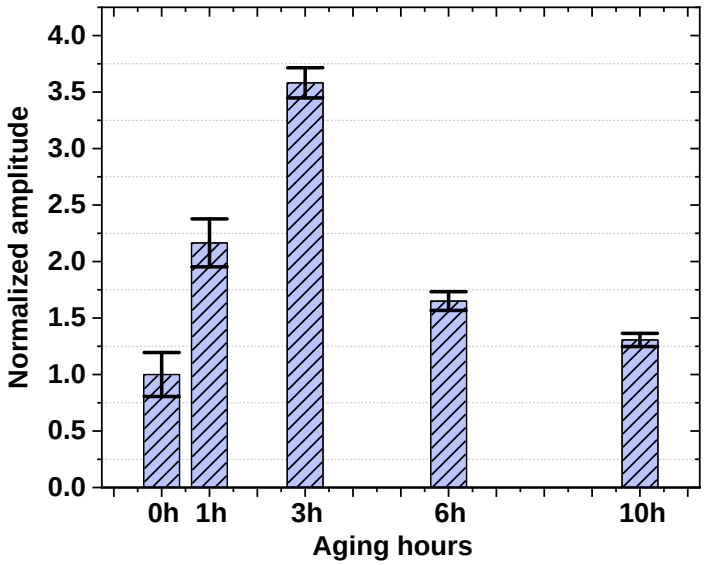

(a)

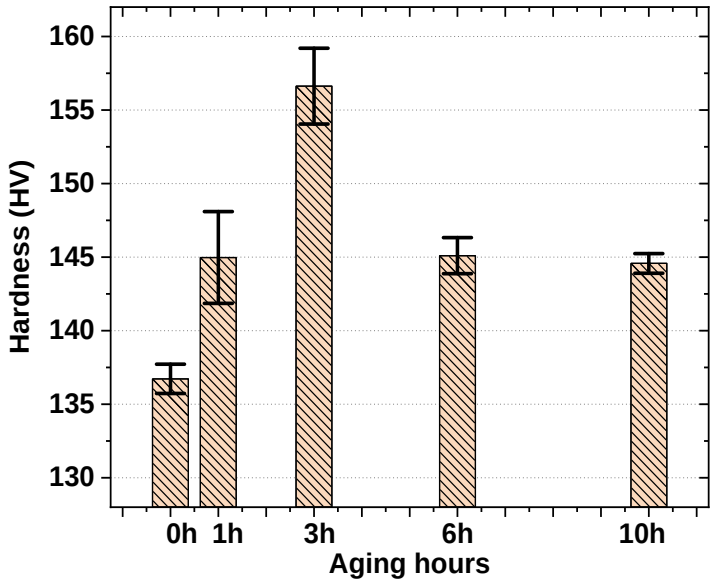

(b)

Figure 7. Variations of (a) third SH harmonic amplitudes and (b) Vickers hardness in the designed thermal aging scheme.

To verify the detected variation trend from the 3rd SH waves, a Vickers hardness test is carried out, with results shown in Fig. 7(b). The aging-hardening phenomenon happens during the first 3 hours heating, reaching a peak value of 156.63 from the initial value of 137 corresponding to the intact status of the plate. After that, a reduction in the hardness indicates that the material begins the over-aging stage. The hardness of the aging specimen after 10 hours then approaches 144.58, which is close to that of the 6-hour aging treatment, suggesting that the microstructures of the material indeed become stable during the last 4 hours of the heating process. By comparing Figs. 7(a) and (b), it can be seen the variation pattern of the Vickers hardness is in perfect agreement with that of the 3rd SH wave

amplitude, thus validating the efficacy and the accuracy of the 3rd SH waves for the monitoring of microstructural changes inside metallic materials.

CONCLUSIONS

In this work, the 3rd SH waves are systematically investigated in views of their applications for material degradation monitoring, exemplified by thermal-aged microstructural changes. A brief theoretical account is first given to offer an understanding on the underlying mechanism behind the high order harmonic wave generation. Based on this, two mode pairs, including the primary-secondary S0 Lamb wave mode pair and the primary-tertiary SH0 wave mode pair are selected. With both the 3rd SH wave-based SHM system and the 2nd Lamb wave-based SHM system installed on the same 2024-T3 aluminum plate, the sensitivity of these two types of nonlinear guided wave methods to thermal-aging-induced microstructural changes is assessed and compared. After that, the 3rd SH waves are applied to monitor the evolution of the material degradations in a plate subjected to a tactically designed thermal aging treatment. Tests results are then verified by a Vickers hardness test.

As a result of changes in the material microstructures due to the thermal aging treatment, comparative experimental results show that the 3rd SH wave amplitude experiences a drastic change while little changes can be observed in the 2nd Lamb wave amplitudes. This demonstrates the higher sensitivity of the 3rd SH waves over the 2nd Lamb waves. As an application example, additional experiments also show that the variation pattern of the 3rd SH amplitude agrees well with that of the Vickers hardness test results at

different heating stages, confirming the reliability and accuracy of the 3rd SH waves in delineating material microstructural changes inside metallic structures.

As a final remark, the presented findings enrich the existing knowledge on microstructure characterization techniques using the 3rd SH waves. With a proper system design to mitigate non-damage-related nonlinear interference, such a technique can be readily applied to realize the incipient damage detection with high sensitivity and fidelity.

ACKNOWLEDGMENTS

The project was supported by grants from the Research Grants Council of Hong Kong Special Administrative Region (PolyU 152070/16E), the National Natural Science Foundations of China through SHENG project (Polish-Chinese Funding Initiative, 51961135302) and the Innovation and Technology Commission of the HKSAR Government to the Hong Kong Branch of National Rail Transit Electrification and Automation Engineering Technology Research Center. The authors would like to acknowledge Prof Zhifeng Tang from Zhejiang University for providing us with the iron-cobalt foil made by his group.

APPENDIX

During the thermal aging process, dislocation dipoles are produced to dramatically change the microstructure and the mechanical properties of a metallic material [26]. A generic one-dimensional Cauchy stress-dislocation dipole interaction model is developed to link up material microstructures to the material nonlinear stress-strain relationship. For simplicity, only normal stress is used in the theoretical analysis, following the common practice widely adopted in the literature [27-28].

When a normal stress perturbation σ is applied in a dislocation dipole zone, the generated total strain ε writes,

$$\varepsilon = \varepsilon_e + \varepsilon_{pl}\,, \tag{A.1}$$

in which ε_e and ε_{pl} are elastic and plastic components associated with the dislocation motion in the dipole configuration, respectively [29]. By extending the nonlinear Hooke's law to the third order, σ and ε_e are linked up by,

$$\sigma = H_2^e \varepsilon_e + \frac{1}{2} H_3^e \varepsilon_e^{\,2} + \frac{1}{3} H_4^e \varepsilon_e^{\,3} + \cdots, \tag{A.2}$$

where H_2^e, H_3^e and H_4^e denote Huang coefficients.

The dislocation dipolar force per unit length F_x along the glide path (shear force per unit length) is given by [30],

$$F_x = -\frac{G\boldsymbol{b}^2}{2\pi(1-\nu)} \frac{x\left(x^2-y^2\right)}{\left(x^2+y^2\right)^2}\,, \tag{A.3}$$

where G, $\boldsymbol{b}$ and ν are the shear modulus, Burgers vector and Poisson's ratio, respectively. For simplicity, Eq. (A.3) assumes that $x = \pm y = \pm h$. To facilitate the derivation, the following equations are required [29],

$$V_x = \boldsymbol{b} R \sigma , \tag{A.4a}$$

$$F_x + V_x = 0 , \tag{A.4b}$$

$$\varepsilon_{pl} = \Omega \Lambda_{dp} \boldsymbol{b} \varsigma , \tag{A.4c}$$

$$\varsigma = \left(x - h \right), \tag{A.4d}$$

where V_x is the shear force per unit length; R the Schmid factor; Ω the conversion factor; Λ_{dp} the dislocation dipole density which is an indicator of the damage level; ς the relative dislocation displacement and h the dipole height. Through a power series expansion of Eq. (A3), and combining Eqs. (A.4), one can obtain the stress perturbation in terms of the variable plastic strain as,

$$\sigma = H_2^{dp} \varepsilon_{pl} + \frac{1}{2} H_3^{dp} {\varepsilon_{pl}}^2 + \frac{1}{3} H_4^{dp} {\varepsilon_{pl}}^3 + \cdots . \tag{A.5}$$

where,

$$\begin{aligned} H_2^{dp} &= \frac{G}{4\pi R \Omega \Lambda_{dp} \left(1-\nu\right) h^2} \\ H_3^{dp} &= \frac{G}{4\pi R \Omega^2 {\Lambda_{dp}}^2 b \left(1-\nu\right) h^3} \\ H_4^{dp} &= \frac{3G}{8\pi R \Omega^3 {\Lambda_{dp}}^3 b^2 \left(1-\nu\right) h^4} \end{aligned} . \tag{A.6}$$

The inverse relations of Eq. (A.2) and Eq. (A.5) are substituted into Eq. (A.1) yields,

$$\varepsilon = \varepsilon_e + \varepsilon_{pl} = \left(\frac{1}{H_2^e} + \frac{1}{H_2^{dp}} \right) \sigma - \left(\frac{\frac{1}{2} H_3^e}{\left(H_2^e \right)^3} + \frac{\frac{1}{2} H_3^{dp}}{\left(H_2^{dp} \right)^3} \right) \sigma^2 + \left(\frac{\frac{1}{2} \left(H_3^e \right)^2 - \frac{1}{3} H_2^e H_4^e}{\left(H_2^e \right)^5} + \frac{\frac{1}{2} \left(H_3^{dp} \right)^2 - \frac{1}{3} H_2^{dp} H_4^{dp}}{\left(H_2^{dp} \right)^5} \right) \sigma^3 + \cdots \quad . \tag{A.7}$$

Taking the inverse relation of Eq. (A.7) and assuming $H_2^{dp} \gg H_2^e$ [29], the material nonlinear stress-strain relationship can be approximated as,

$$\sigma = A_2^e \varepsilon + \beta \varepsilon^2 + \gamma \varepsilon^3 + \cdots, \tag{A.8}$$

where

$$\beta = -\frac{H_3^e}{2} + \frac{8\pi^2 R^2 \Omega \Lambda_{dp} h^3 \left(1-\nu\right)^2 \left(H_2^e \right)^3}{G^2 b}$$

$$\gamma = \frac{H_4^e}{2} + \frac{192\pi^4 R^4 \Omega^2 {\Lambda_{dp}}^2 h^6 \left(1-\nu\right)^4 \left(H_2^e \right)^5}{G^4 b^2} - \frac{96\pi^3 R^3 \Omega \Lambda_{dp} h^4 \left(1-\nu\right)^3 \left(H_2^e \right)^4}{G^3 b^2} - \frac{24\pi^2 R^2 \Omega \Lambda_{dp} h^3 \left(1-\nu\right)^2 \left(H_2^e \right)^2 H_3^e}{G^2 b} \quad , \tag{A.9}$$

in which β and γ are defined as the third-order and the fourth-order elastic constants, respectively. Eq. (A.8) depicts the generation of the total strain with the first, second- and third-order components due to the interaction of the dislocation dipoles with the perturbation stress in the material. It can be found from Eq. (A.9) that γ is highly depended on both Λ_{dp} term and ${\Lambda_{dp}}^2$ term but β only depended on Λ_{dp} term. For a given variation of the dislocation dipole density, the fourth-order elastic constant should be more sensitive than the third-order elastic constant.

REFERENCES

1. Chang F K, Markmiller J F C and Yang J, et al. Structural health monitoring. *System Health Management: With Aerospace Applications.* Wiley, 2011, pp.419-428.
2. Giurgiutiu V. *Structural Health Monitoring with Piezoelectric Wafer Active Sensors*. 2nd ed. New York: Academic, 2014.
3. Raghavan A, Cesnik C E. Review of guided-wave structural health monitoring. *Shock Vib.* 2007; 39(2): 91-116.
4. Meeker T, Meitzler A. Guided wave propagation in elongated cylinders and plates. *Phys. Acoust*. 1964; 1 (Part A): 111-167.
5. Chillara V K and Lissenden C J. Review of nonlinear ultrasonic guided wave nondestructive evaluation: theory, numerics, and experiments. *Opt. Eng.* 2015; 55 (1): 011002.
6. Matlack K, Kim J-Y and Jacobs L, et al. Review of second harmonic generation measurement techniques for material state determination in metals. *J. Nondestruct. Eval.* 2015; 34: 273.
7. Roy S, Lonkar K and Janapati V, et al. A novel physics-based temperature compensation model for structural health monitoring using ultrasonic guided waves. *Struct. Health Monit.* 2014; 13 (3): 321-342.
8. Masserey B and Fromme P. Fatigue Crack growth monitoring using high-frequency guided waves. *Struct. Health Monit.* 2013; 12(5-6): 484-493.
9. Deng M and Pei J. Assessment of accumulated fatigue damage in solid plates using nonlinear Lamb wave approach. *Appl. Phys. Lett.* 2007; 90: 121902.

10. Pruell C, Kim J-Y and Qu J, et al. Evaluation of plasticity driven material damage using Lamb waves. *Appl. Phys. Lett*. 2007; 91(23): 231911.
11. Xiang Y, Xuan F and Deng M. Evaluation of thermal degradation induced material damage using nonlinear Lamb waves. *Chin. Phys. Lett.* 2010; 27(1): 016202.
12. Chillara V K and Lissenden C J. Interaction of guided wave modes in isotropic weakly nonlinear elastic plates: Higher harmonic generation. *J. Appl. Phys.* 2012; 111(12): 124909.
13. Liu Y, Lissenden C J and Rose J L. Microstructural characterization in plates using guided wave third harmonic generation. *AIP Conf. Proc.* 2014; 1581(1): 639-645.
14. Liu Y, Chillara V K and Lissenden C J. Third harmonic shear horizontal and Rayleigh Lamb waves in weakly nonlinear plates. *J. Appl. Phys.* 2013; 114(11):114908.
15. Lissenden C J, Liu Y and Choi G. Effect of localized microstructure evolution on higher harmonic generation of guided waves. *J. Nondestruct. Eval.* 2014; 33(2):178-186.
16. Shan S, Cheng L and Wen F. Design of nonlinear-Lamb-wave-based structural health monitoring systems with mitigated adhesive nonlinearity. *Smart Mater. Struct.* 2018; 27(10): 105006.
17. Shan S and Cheng L. Mixed third harmonic shear horizontal wave generation: interaction between primary shear horizontal wave and second harmonic Lamb wave. *Smart Mater. Struct*. 2019; 28: 8.
18. Lin Y, Xia Y and Jiang Y, et al. Precipitation hardening of 2024-T3 aluminum alloy during creep aging. *Mater. Sci. Eng. A.*2013; 565: 420-429.
19. Kostorz G. X-ray and neutron scattering. In: Cahn RW, Hassen P (eds). *Physical Metallurgy*. 3rd ed Amsterdam: North-Holland, 1983, p.793.

20. Cantrell J H and Yost W T. Determination of precipitation nucleation and growth rates from ultrasonic harmonic generation. *Appl. Phys. Lett. 2000;* 77(13): 1952-1954.
21. Shan S. *Nonlinear guided-wave-based structural health monitoring: mechanism and system design for material degradation monitoring*. PhD Thesis, The Hong Kong Polytechnic University, HK, 2019.
22. Shan S, Cheng L and Li P. Adhesive nonlinearity in Lamb-wave-based structural health monitoring systems. *Smart Mater. Struct.* 2016; 26(2): 025019.
23. Hasanian M and Lissenden C J. Second order harmonic guided wave mutual interactions in plate: Vector analysis, numerical simulation, and experimental results. *J. Appl. Phys*. 2017; 122(8): 084901.
24. Shan S, Cheng L and Wen F. Design of nonlinear-Lamb-wave-based structural health monitoring systems with mitigated adhesive nonlinearity. *Smart Mater. Struct.* 2018; 27(10): 105006.
25. Hasanian M and Lissenden C J. Second order harmonic guided wave mutual interactions in plate: Vector analysis, numerical simulation, and experimental results. *J. Appl. Phys*. 2017; 122(8): 084901.
26. Zhou Q, Wang J and Misra A, et al. Dislocations interaction induced structural instability in intermetallic Al_2Cu. *Npj Comput. Mater*. 2017; 3: 24.
27. Xiang Y, Deng M and Xuan F. Creep damage characterization using nonlinear ultrasonic guided wave method: A mesoscale model. *J. Appl. Phys*. 2014; 115: 044914.
28. Zhao Y, Qiu Y and Jacobs L J, et al. A micromechanics model for the acoustic nonlinearity parameter in solids with distributed microcracks. *AIP Conf. Proc.* 2016; 1706: 060001.

29. Cantrell J H and Yost W T. Nonlinear ultrasonic characterization of fatigue microstructures. *Int. J. Fatigue* 2001; 23(1): 487-490.

30. Hull D and Bacon D J. *Introduction to dislocations*. Oxford: Pergamon, 1984, p.77.